Published in final edited form as:
*Neuroimage*. 2014 January 15; 85(0 1): . doi:10.1016/j.neuroimage.2013.05.034.

# Probing the early development of visual working memory capacity with functional near-infrared spectroscopy

**Aaron T. Buss**[1], **Nicholas Fox**[1], **David A. Boas**[2], and **John P. Spencer**[1,*]

[1]Department of Psychology and Delta Center, University of Iowa

[2]Massachusetts General Hospital and Harvard Medical School

## Abstract

Visual working memory (VWM) is a core cognitive system with a highly limited capacity. The present study is the first to examine VWM capacity limits in early development using functional neuroimaging. We recorded optical neuroimaging data while 3- and 4-year-olds completed a change detection task where they detected changes in the shapes of objects after a brief delay. Near-infrared sources and detectors were placed over the following 10–20 positions: F3 and F5 in left frontal cortex, F4 and F6 in right frontal cortex, P3 and P5 in left parietal cortex, and P4 and P6 in right parietal cortex. The first question was whether we would see robust task-specific activation of the frontal-parietal network identified in the adult fMRI literature. This was indeed the case: three left frontal channels and 11 of 12 parietal channels showed a statistically robust difference between the concentration of oxygenated and deoxygenated hemoglobin following the presentation of the sample array. Moreover, four channels in the left hemisphere near P3, P5, and F5 showed a robust increase as the working memory load increased from 1–3 items. Notably, the hemodynamic response did not asymptote at 1–2 items as expected from previous fMRI studies with adults. Finally, 4-year-olds showed a more robust parietal response relative to 3-year-olds, and an increasing sensitivity to the memory load manipulation. These results demonstrate that fNIRS is an effective tool to study the neural processes that underlie the early development of VWM capacity.

### Keywords

visual working memory; functional neuroimaging; development; working memory capacity; near-infrared spectroscopy

## 1. Introduction

Working memory has been called the heart of intelligent behavior (Nę cka, 1992), and a core property of this cognitive system is its highly limited capacity. Working memory capacity limitations are reliably predictive of individual differences in a host of cognitive functions including fluid intelligence, language comprehension, and scholastic achievement (e.g., Conway, Kane, & Engle, 2003). This predictive relationship appears to be particularly strong for visual working memory (VWM). VWM plays a key role in much of visual



*Corresponding author: john-spencer@uiowa.edu.

cognition, comparing percepts that cannot be simultaneously foveated and identifying changes in the world when they occur (for review, see Luck & Vogel, 1997; Vogel, Woodman, & Luck, 2001). By some estimates, individual differences in VWM capacity account for up to 40% of the variance in global fluid intelligence (Fukuda, Vogel, Mayr, & Awh, 2010). VWM capacity limitations also have a profound influence on cognitive development across a range of domains (e.g., Oakes, Horst, Kovack-Lesh, & Perone, 2008), and visuo-spatial WM deficits have been observed in clinical populations, including children diagnosed with attention-deficit/hyperactivity disorder (ADHD; Willcutt, Doyle, Nigg, Faraone, & Pennington, 2005), autism (Steele, Minshew, Luna, & Sweeney, 2007), developmental coordination disorder (Alloway, 2007), and schizophrenia (Cullen et al., 2010), as well as children born preterm (Vicari, Caravale, Carlesimo, Casadei, & Allemand, 2004). Given these pervasive influences, understanding the development of VWM and the nature of VWM capacity limits has broad implications and may be central to developing early interventions for atypically developing populations.

The method of choice for probing VWM capacity is the change detection task (Luck & Vogel, 1997). Here, participants are shown a memory array (100–500 ms), there is a brief delay (250–1000 ms), and then a test array appears in which either all of the objects match the memory array, or the feature(s) of one object is changed to a new value. Participants report whether they detected a change in the second array or whether the arrays were the same. This task has several advantages over other visuo-spatial tasks. For instance, the brief presentation and short delay reduces the likelihood of verbal recoding and rehearsal (Vogel et al., 2001), and location is typically not a relevant dimension in the task—items in both arrays are generally in the same positions—so the influence of spatial memory is minimized. Thus, change detection provides a relatively direct probe of the VWM system.

Recent work using fMRI has revealed a distributed network of frontal and posterior cortical regions that underlies VWM and change detection. VWM representations are actively maintained in the intraparietal sulcus (IPS), the dorso-lateral prefrontal cortex (DLPFC), the ventral-occipital (VO) cortex for color stimuli, and the lateral-occipital complex (LOC) for shape stimuli (Todd & Marois, 2005; 2004). Many of these regions show a key signature of VWM capacity: the BOLD signal increases as more items must be remembered, and this increase asymptotes near the capacity of the VWM system. For instance, Todd and Marois (2004) reported an increase in the BOLD signal in IPS as the number of items in the change detection task (the set size) increased from 1 to 3. This neural signal reached an asymptote at set sizes 4, 6, and 8, consistent with behavioral estimates of VWM capacity using Pashler's capacity measure, *k* (Pashler, 1988). Other data have revealed a suppression of the temporo-parietal junction (TPJ) during the delay interval of the change detection task (Todd, Fougnie, & Marois, 2005), and activation of the anterior cingulate cortex (ACC) during the comparison phase (Mitchell & Cusack, 2007; Todd et al., 2005). Moreover, there is greater activation of this network on change versus no change trials, and the hemodynamic response on error trials tends to be less robust (Pessoa & Ungerleider, 2004; Pessoa, Gutierrez, Bandettini, & Ungerleider, 2002).

Developmental studies using the change detection task have revealed that 3-year-olds have a capacity between 1.5 and 2 items (Simmering, 2012). Capacity increases to 2–3 items by 5 years and to roughly 4 items by 7 years (Cowan et al., 2005; Riggs, McTaggart, Simpson, & Freeman, 2006; Simmering, 2012). What neural systems underlie these changes in VWM capacity? Previous studies have reported activation across frontal (DLPFC, VLPFC) and parietal (intra and inferior parietal regions) regions in VWM tasks across a range of ages from 6 to 23 years (Bunge & Wright, 2007; Edin, Macoveanu, Olesen, Tegnér, & Klingberg, 2007; Fair et al., 2007; Geier, Garver, Terwilliger, & Luna, 2009; Klingberg, Forssberg, & Westerberg, 2002; Klingberg, 2006; Kwon, Reiss, & Menon, 2002; Nelson et al., 2000;

Olesen, Macoveanu, Tegnér, & Klingberg, 2007; Scherf, Sweeney, & Luna, 2006; Thomas et al., 1999; Vuontela et al., 2009). Frontal-parietal activation becomes stronger (Kwon et al., 2002; Olesen et al., 2007; Thomas et al., 1999) and, in some cases, more localized (Geier et al., 2009; Scherf et al., 2006) over development. Additionally, some studies have reported involvement of the caudate nucleus (Bunge & Wright, 2007; Olesen et al., 2007; Scherf et al., 2006), precuneus (Scherf et al., 2006), and parts of the premotor cortex (Scherf et al., 2006; Thomas et al., 1999) in VWM tasks, but these effects have been inconsistent across age groups. Finally, several studies reported a decrease in the activation of Broca's area as a function of age which may be linked to verbal reasoning strategies employed by children during the task (Kwon et al., 2002).

Although these data have shed light on the neural systems that underlie changes in VWM over development, technical barriers have prevented an extension of this work into early development. fMRI is extremely sensitive to movement of the head—an obvious limitation when working with infants and young children—and the background noise created by MRI is quite loud. Such technical barriers are unfortunate given that individual differences in cognitive performance in the first two years of life are predictive of later performance (Rose, Feldman, & Jankowski, 2009; 2012), and recent analyses suggesting that investments and intervention efforts in early development are among the wisest (Heckman, 2006).

An alternative to fMRI is to use functional Near-Infrared Spectroscopy. fNIRS uses light in the near infrared range (695–1000 nm) which passes through the skull and brain tissue. fNIRS systems measure the absorption and scattering of photons as light passes through, allowing for the quantitative measurement of changes in cerebral blood volume and oxygenation resulting from functional activation. Because fNIRS uses light-weight and quiet light emitters and receivers directly attached to the head, this technology is much more resistant to head movements. With respect to spatial resolution, fNIRS is better than EEG but poorer than fMRI. Its greatest limitation is its inability to examine relatively deep areas of the cortex (infrared light generally penetrates up to 2 cm into the brain depending on the separation between the source and the detector). Given that infants and young children have relatively thin skulls and small brains, however, this limitation is much less severe. Moreover, a large proportion of the frontal-parietal network central to VWM is located close to the cortical surface and can be measured using fNIRS even with adults (Cutini et al., 2011). Thus, fNIRS is ideally suited as a cognitive neuroscientific technique to study the VWM system early in development (Aslin & Mehler, 2005).

In this report, we present data from the first functional neuroimaging study to examine the neural basis of VWM capacity in early development. Three- and 4-year-old children participated in a change detection task where we varied the number of items they had to remember from 1 item to 3 items while we simultaneously recorded neural activity using a 24-channel fNIRS system with sources and detectors positioned over frontal and parietal cortical areas in both the left and right hemispheres. Our central question was whether the frontal-parietal network identified using fMRI would show task-specific neural activity, and how this network would change between 3 and 4 years. We also examined whether the same neural signature of VWM capacity—the asymptote of neural activity at capacity (Todd & Marois, 2004)—would be evident early in development.

## 2. Method

### 2.1. Participants

Twenty-eight 3.5-year-olds (17 females; *M* age = 3.5 years, *SD* = 1.5 months) and 19 4.5-year-olds (7 females; *M* age = 4.5 years, *SD* = 2.5 months) participated in the two-session study. Children were recruited from a participant registry maintained by the Department of

Psychology. Parents were sent a letter inviting them to participate and then received a follow-up phone call. All children had normal or corrected-to-normal vision. Seven children were Asian or African-American; the remaining participants were Caucasian. Nine additional 3.5-year-olds were enrolled in the study but were excluded from further analysis: 6 completed only one session, 2 had noisy NIRS signals, and 1 took the NIRS cap off during a session. Two additional 4.5-year-olds were enrolled in the study but were excluded from further analysis because they only completed one session.

The final sample contributing behavioral data included 18 3.5-year-olds and 18 4.5-year-olds. As we discuss below, several children were excluded from the behavioral analysis for poor behavioral performance (<50% correct on set size 1 trials for 2 or more runs). fNIRS data from 3 additional 3.5-year-olds and 1 additional 4.5-year-old were excluded from fNIRS analyses after motion-rejection and outlier removal because they failed to contribute data to every cell in the experimental design (see below).

### 2.2. Stimuli and apparatus

We used the change detection task from Simmering (2012). The task was explained to children using 3 × 3 inch flashcards that contained a set size of 1 (SS1), 2, or 3 items. The task proper was completed on a 46 inch LCD television monitor that was connected to a PC running E-Prime 2.0 software (Psychology Software Tools, Pittsburgh, PA). Children were seated approximately 25 inches from the screen. The stimulus arrays were composed of a subset of 8 different white shapes (see Figure 1) presented on a virtual grey card on a black background. The shapes subtended approximately 1 by 1 inch and the virtual grey card subtended a 6.25 by 6.25 inch area. Shapes were presented in any of six randomly selected and evenly spaced locations 3 inches from the center of the grey rectangle. On a given trial, an array of 1 to 3 items was presented. On same trials, the second array contained the same shapes in the same configuration as the sample array. On a change trial, the second array contained a new shape at a location previously occupied on the sample array.

### 2.3. Procedure and design

At the start of the first session, an experimenter described the task to the child as a ‘matching’ game. The experimenter first demonstrated the task using the flash cards which were placed on a large piece of black cardstock that was positioned in front of the child. The flash cards were placed on the left or right side of the cardstock in an alternating fashion from one trial to the next. The first card was shown for approximately 2 seconds and the child was instructed to look at the picture and remember the shapes. The first card was then removed, and after a brief delay the second card was placed in the same location as the first card. The experimenter then asked the child if the two pictures matched. After the child responded, the experimenter placed both cards side by side and corrected the child as needed, pointing out the changed item when relevant to ensure the child understood the proper comparison. Participants completed 3 of these practice trials (one at each SS) with the flashcards. If the child failed to answer the sample questions correctly or failed to point out the change on change examples, we re-explained the task, highlighting the goals of the game. Note that this was an informal assessment since some children are not very verbal in the laboratory. Thus, if the experimenter was unsure that the child understood the task, the experimenter spent some extra time re-explaining the task a second time.

After the instruction phase, the experimenter began the computerized version. There were 4 additional practice trials at the beginning of the computerized version (SS2 change, SS3 same, SS1 change, SS2 same). Each trial began with an auditory prompt saying, “*Let’s look for shape changes!*” along with a grey fixation circle centered on the side of the screen on which the next trial would occur. Once the child was oriented to the appropriate side of the

screen, the experimenter pressed a button on the keyboard to initiate the trial. The sample array was then presented for 2 seconds, after which the screen was blanked for 1 second. The test array was then displayed until a response was given (see Figure 2). Children gave a verbal response of 'match' or 'no match' which the experimenter then entered on the keyboard. We asked children to respond verbally because pushing response keys was too demanding. Three-year-olds typically responded within 5 seconds after the appearance of the test array (*M* response time = 5.0 s, *SD* = 1.4s). Four-year-olds typically responded within 3 seconds (*M* = 3.8 s, *SD* = .97 s). Note that these values include the reaction time of the experimenter. The delay between trials was jittered at 1, 2, or 4 seconds selected in a 2:1:1 ratio. The fixation circle was then presented on the other side of the screen along with the auditory prompt to begin the next trial.

Children completed four runs through the event-related task design split over two visits to the laboratory (2 runs per session). Each run consisted of 12 trials (6 same, 6 changed randomized from trial to trial) at each set size (presented in the order SS1, SS2, and SS3). Sessions were separated by an average of 7.5 days. Practice with the flashcards was administered at the beginning of each session to ensure that they remembered the goals of the task. Moreover, computerized practice trials were administered on the first run of each session.

### 2.4. NIRS data acquisition

NIRS data were collected at 25 Hz using a 24-channel TechEn CW6 system with wavelengths of 830 nm and 690 nm. Light was delivered via fiber optic cables that terminated in a customized cap (Figure 3) placed on the head with sources and detectors secured within four flexible plastic arrays. Each array contained 2 sources and 4 detectors placed 3 cm apart creating 6-channel arrays with foam padding underneath to ensure that they would rest comfortably on the head. These arrays were placed on the head relative to the 10–20 system with one array placed over the left frontal cortex (over F3-F5), a second array over the right frontal cortex (over F4-F6), a third array placed over the left parietal cortex (over P3-P5), and a fourth array placed over the right parietal cortex (over P4-P6). Figure 4 shows the placement of the arrays on a model head created by digitizing the optode positions on a sample participant using a Polhemus motion-tracking system. NIRS data were time-stamped at the onset of the sample array on each trial through synchronization with the computer running the experiment using E-Prime software.

### 2.5. NIRS data processing

One approach to analyzing NIRS data is to only include participants who contribute data for all NIRS channels and all conditions; examination of our data, however, revealed that this was not ideal. For instance, motion artifact appeared to impact signals locally (e.g., near F5) rather than globally. Thus, we had to exclude different numbers of trials over different cortical regions for each participant. Thus, we split the NIRS data into 8 regions composed of 3-channel sets depicted in Figure 4 and allowed different participants to contribute data for each region. We will refer to these 3-channel sets using the 10–20 sites they were placed over and the channel number moving from the front of the head to the back. For instance, the 3 channel array near F5 will be referred to as F5-1, F5-2, and F5-3.

Using HomER2 software (Huppert, Diamond, Franceschini, & Boas, 2009), data were first demeaned and converted into an optical density measure. Next, the data were band-pass filtered to remove frequencies slower than .016 Hz and faster than 2 Hz. Motion artifacts were then removed from each region by eliminating trials with a change in optical density larger than 0.35 absorbance units within the time window between 2 seconds before to 12 seconds after the onset of the sample array. Motion artifacts were typically caused by large

movements of the head and body; we saw no evidence that children's verbal responses created motion artifacts. Data were then band-pass filtered again to retain only frequencies between .016 and .5 Hz. Concentration data were computed using the modified Beer-Lambert Law and the known extinction coefficients of oxygenated and deoxygenated hemoglobin (Boas et al., 2001). Finally, outlier trials were removed that contained amplitudes of oxy-Hb that were more than 2.5 standard deviations above or below a participant's mean in each condition for 9 consecutive time-samples (a duration of 360 ms). Outliers were only removed from channels and conditions for which a robust estimate of the mean could be obtained. Thus, participants had to contribute a minimum of 5 trials in order to perform outlier removal for a given condition in a given region.

### 2.6. Method of analysis

To be included in the following analyses, criteria were placed on both the behavioral and fNIRS data. First, children were required to show good behavioral performance and demonstrate that they understood the task. The VWM capacity of 3- and 4-year-olds is typically estimated to be around 1–2 objects (Simmering, 2012); thus, we set a performance criterion using the set size 1 (SS1) trials. Specifically, we only included children who performed above 50% at SS1 for at least 3 runs. Eleven (10 3-year-olds) children were excluded from analyses for this reason, leaving a total of 18 3-year-olds and 18 4-year-olds that were included in the behavioral data analysis. We analyze the behavioral data using % correct and the maximum estimate of capacity (Pashler's *k*; Pashler, 1988) across set-sizes. Pasher's *k* is computed using equation 1, where S is the set-size, H is the rate of hits, and g is an estimate of guessing (which is calculated as 1 – false-alarms).

$$k=S^{*}(H-g)/(1-g) \quad (1)$$

The fNIRS analyses only focus on correct trials and additional criteria were placed on inclusion in the fNIRS dataset. A participant's data were only included in a region's analysis if the participant contributed data to all 6 trial types (SS 1–3 × Same/Different Correct). Four additional participants (3 3-year-olds) were not included in the final fNIRS analyses because they either contributed data for only one region (2 participants) or they failed to contribute neural data to any region. This left 15 3-year-olds and 17 4-year-olds who contributed data to the fNIRS analysis. Table 1 displays the number of participants, average trial counts, and the percent of included trials for each condition and region. Trials that were eliminated from the fNIRS data were lost due to motion rejection or removal of outlier trials. In all cases, the average number of trials that were retained was high, allowing for robust estimates of children's hemodynamic responses.

Given that the number of trials varied by participant in each region, we computed a weighted mean for each participant where the average hemodynamic response ($HbO_2$, HbR) was weighted by the number of trials. This reduced the possibility that statistically significant effects might be driven primarily by participants with few trials. For statistical analyses, the mean weighted average was computed within an 'early' phase that was 4–7 seconds after the presentation of the sample array and a 'late' phase that was 7–10 seconds after the presentation of the sample array. Note that because the test array was presented 3 seconds after the sample array, the 'late' phase was 4–7 seconds after the presentation of the test array. The early phase was chosen to capture the peak response to the onset of the sample array, while the late phase was chosen to capture the peak response to the onset of the test array and the generation of a same/different decision. In studies of visual working memory with adults, the hemodynamic response typically reaches its maximum 6 seconds after stimulus presentation (e.g., Harrison, Jolicoeur, & Marois, 2010; Todd & Marois, 2004). Less is known about the timing of the hemodynamic response with young children,

although there are several reports with older children. For instance, Schroeter and colleagues (2004) reported a peak hemodynamic response 7–8 seconds post-stimulus in a Stroop task with 7 to 13-year-olds. Based on these data, we assumed that the hemodynamic response would peak about 7 s post-stimulus. Critically, the 4–7 second post-stimulus time window ensured that we had non-overlapping averages[1].

## 3. Results

### 3.1. Behavioral results

Figure 5 shows the decline in children's performance as the set size (SS) varied from one to three items. These data were analyzed in a two-way ANOVA with SS as a within-subjects factor and Age as a between-subjects factor. There was a significant decline in performance over SS, $F(2,33) = 86.85$, $p < .001$, and 4-year-olds had a significantly higher percent correct than 3- year-olds, $F(1,34) = 26.28$, $p < .001$. The interaction of these factors was not significant. We also calculated the maximum capacity of each child's performance using Pashler's *k*. A t-test indicated that 4-year-olds had a higher capacity ($M = 1.73$) than 3-year-olds ($M = 1.30$), $t(34) = -2.6$, $p < .05$.

### 3.2. fNIRS results

The weighted means from each fNIRS channel were analyzed in an Age (3yo, 4yo) × SS (1, 2, 3 items) × Phase (early: 4–7s, late: 7–10s) repeated measures ANOVA with Age as a between-subjects factor and SS and Phase as within-subjects factors. We also included an additional within-subjects contrast in the ANOVA comparing the concentration of oxy-Hb ($HbO_2$) to deoxy-Hb (HbR). Oxy-Hb and deoxy-Hb typically show an inverse relationship[2] (see, Huppert, Hoge, Diamond, Franceschini, & Boas, 2006), and the assumption of a negative correlation between oxy-Hb and deoxy-Hb has proven to be an effective way to reduce noise in fNIRS analyses (Cui, Bray, & Reiss, 2010). Inspection of our data revealed that oxy-Hb and deoxy-Hb showed the canonical pattern. Thus, we used the HbX contrast as a gateway comparison, that is, only channels with a significant HbX effect ($HbO_2 \neq HbR$) were included in follow-up analyses[3]. A significant HbX effect (main effect or interaction) indicates that (1) a channel had a high enough signal-to-noise ratio to detect a difference in the concentration of oxy-Hb and deoxy-Hb, and (2) there was a robust task-related neural response in the cortical region underlying this channel (i.e., the hemodynamic response was statistically robust during the 4–10 s event window). Note that we used multivariate statistics (Wilks' $\Lambda$) for all within-subjects effects because such tests do not require the assumption of sphericity.

We report results of the ANOVAs in the following three sections. In the first section, we highlight robust HbX or HbX × Phase effects that did not otherwise interact with SS or Age. To preview our results, we found robust, task-related neural responses in 11 of 12 parietal channels and 3 left frontal channels. Next, we report all SS-related effects (that did not otherwise interact with Age) for all channels that passed the gateway comparison (i.e., channels with a statistically robust difference between the concentration of oxy-Hb and

[1]Although we included Phase ('early', 'late') as a factor in the ANOVAs reported in the Results, it is worth noting that the absence of an early/late difference would not preclude the detection of a robust hemodynamic that, say, peaked at 8 s, because we also included a second contrast between oxy-Hb and deoxy-Hb (see Results).

[2]Several studies have reported negative functional responses as well as positive and biphasic responses with newborns and infants (Lloyd-Fox, Blasi, & Elwell, 2010; Seghier, Lazeyras, & Huppi, 2006; Wolf & Greisen, 2009). These results are controversial, with on-going debates about the origin of such signals (Roche-Labarbe et al., 2013). Critically, this controversy is confined to infancy and pathological cases. We know of no reports of negative or biphasic and positive responses with children.

[3]Data from only one channel were influenced by this gateway criterion, that is, only one channel showed a significant effect in the absence of an HbX effect. Inspection of these data revealed a noisy hemodynamic response, suggesting that the gateway criterion was effective.

deoxy-Hb). Four parietal channels and one left frontal channel showed robust SS effects. Finally, we report all Age-related effects for all channels that passed the gateway comparison. Three parietal channels and one right frontal channel showed robust Age effects. In each section, we follow-up the highest level interaction for each channel using tests of simple effects. These tests explore the nature of the interaction by examining differences among groups within one factor for each level of another factor. The advantage of simple effects tests over t-tests is that they provide a more robust estimate of the error term because they use the within-cell variance for all cases included in the follow-up analysis (for discussion, see Green, Salkind, & Akey, 1997; Harris, 1985; Howell, 1992).

**3.2.1. HbX effects—**Figure 6 shows the hemodynamic response for all channels with statistically significant HbX effects ($HbO_2 \neq HbR$), Phase effects (Early ≠ Late), or HbX × Phase interactions (see Table 2 for details). Dark colors show oxy-Hb and light colors show deoxy-Hb. The dark-light color pairs (black, brown, green) show the hemodynamic response from specific channels (see colored channels on the model head). There was a statistically robust difference between the concentration of oxy-Hb and deoxy-Hb in all P3 and P4 channels and P6-1 (see Table 2), with a peak hemodynamic response around 7 s (Figure 6A – 6C). The hemodynamic response for P6-2 was similar (Figure 6A, green lines) except the peak response occurred earlier (around 6 s). Consequently, there was only a significant difference between the concentration of oxy-Hb and deoxy-Hb in the early phase (see Table 2).

The second pattern evident in the data was a shift in the concentration of oxy-Hb across the early to late phases in all three P5 channels and F5-2 (Figure 6D–6E). In particular, the concentration of oxy-Hb was high early and low late leading to a statistically robust difference across phases (Table 2). Note that for two of these channels—P5-2 and P5-3 (green and brown lines in Figure 6D, respectively)—there was also a robust difference between the concentration of oxy-Hb and deoxy-Hb in the early phase (see Table 2). The final pattern evident in three channels—two F3 channels (F3-2, F3-3; see Figure 6F) and P5-2—reflected the opposite pattern in the concentration of deoxy-Hb across phases. Specifically, the concentration of deoxy-Hb was low early and showed a statistically robust increase late (see Table 2).

**3.2.2. SS effects—**Figure 7 shows the hemodynamic response for all channels with statistically significant SS effects (main effects or interactions; see Table 3). Three left parietal channels—P3-2 (Figure 7A), P3-3 (Figure 7B), and P5-3 (Figure 7C)—showed a robust hemodynamic response, particularly at the highest set size (SS3). In particular, tests of simple effects for P3-2 showed a significantly higher concentration of oxy-Hb relative to deoxy-Hb at SS3, $F(1,25) = 4.55$, $p < .05$, and an increase in the hemodynamic response in the late phase at SS3, $F(1,25) = 3.94$, $p = .058$. There were no significant effects at SS1 and SS2 ($p > .1$). Similarly, channel P3-3 showed an increase in the hemodynamic response in the late phase at SS3, $F(1,25) = 3.12$, $p = .089$; no other simple effects tests approached significance ($p > .1$). Finally, channel P5-3 showed a significantly higher concentration of oxy-Hb relative to deoxy-Hb at both SS1, $F(1,22) = 4.39$, $p < .05$, and SS3, $F(1,22) = 7.36$, $p < .05$, but not at SS2 ($p > .1$).

These results showing a robust hemodynamic response at the highest set size in left parietal cortex are consistent with findings from the left frontal cortex (Figure 7D). In particular, tests of simple effects for channel F5-1 (Table 3) showed a significant increase in the concentration of oxy-Hb across set sizes, $F(1,22) = 4.39$, $p < .05$, but no significant change in the concentration of deoxy-Hb ($p > .1$). Additional tests of simple effects indicated that the concentration of oxy-Hb was greater at SS3 versus SS1, $F(1,25) = 13.8$, $p < .001$, with a weaker difference between SS3 and SS2, $F(1,25) = 3.21$, $p = .085$.

The final set size effect diverged from the pattern of results in the left hemisphere: there was a significant SS effect in the right parietal cortex in channel P4-1 (Figure 7E; see Table 3). Tests of simple effects indicated that the hemodynamic response at SS2 was greater than SS1, $F(1,18) = 5.94$, $p < .05$; all other comparisons were non-significant ($p > .1$).

**3.2.3. Age effects—**Figure 8 shows the hemodynamic response for all channels with statistically significant Age effects (main effects or interactions; see Table 4). Four-year-olds showed a more robust hemodynamic response in two parietal channels relative to 3-year-olds. In particular, there was a significant Age main effect in channel P3-1, and significant interactions between Age, Phase, and HbX in P6-3 (Table 4). In the latter case, tests of simple effects showed no significant hemodynamic response for 3-year-olds (all comparisons $p > .1$), while 4-year-olds showed a higher concentration of oxy-Hb relative to deoxy-Hb, $F(1,16) = 5.97$, $p < .05$, and a stronger overall hemodynamic response in the early phase, $F(1,16) = 4.89$, $p < .05$ (see Figure 8A). These two effects interacted as well, $F(1,16) = 5.38$, $p < .05$, yielding a robust difference in the concentration of oxy-Hb and deoxy-Hb in the early phase and a weaker difference in the late phase.

In the left parietal cortex (channel P5-3), the two groups of participants had different hemodynamic responses as the set size increased (Table 4). Tests of simple effects showed a robust SS × Phase interaction for 4-year-olds, $F(2,11) = 5.55$, $p < .05$. Additional tests of simple effects indicated that 4-year-olds' responses differed significantly across set sizes in the late phase, $F(2,11) = 4.72$, $p < .05$, with the strongest hemodynamic response in the late phase at SS3 (see Figure 8B). There were no differences across set size in the early phase for this age group ($p > .1$). This mimics the pattern of set size effects identified in P3-2 and P3-3 (see Figure 7A–7B). Three-year-olds, by contrast, showed only a robust Phase effect, $F(1,10) = 9.86$, $p < .01$, with a high concentration of oxy-Hb early and a decline late (Figure 8C) which mimics the early versus late differences shown in Figure 6D.

Finally, there was a significant 4-way interaction in one right frontal channel (F4-1; see Table 4). Tests of simple effects indicated that there were no significant differences in the concentration of deoxy-Hb in this channel ($p > .1$), but there was a significant SS × Phase × Age interaction in the concentration of oxy-Hb, $F(2,22) = 4.25$, $p < .05$. Additional tests of simple effects showed no significant differences in the concentration of oxy-Hb for 4-year-olds ($p > .1$), while there was a significant SS × Phase interaction for 3-year-olds, $F(2,11) = 11.96$, $p < .01$. Comparisons across phases for each set size showed a robust increase in the concentration of oxy-Hb across phases for SS1, $F(1,12) = 5.59$, $p < .05$, and a robust decrease in the concentration of oxy-Hb across phases for SS3, $F(1,12) = 15.33$, $p < .01$. This latter effect is consistent with the decline in the concentration of oxy-Hb across phases for the 3-year-olds in left parietal cortex (see Figure 8C).

As a final analysis step, we examined whether neural responses from any of the channels showing Age effects were significantly correlated with children's behavioral performance. A regression model with the concentration of oxy-Hb for channel F4-1 at SS3 in the early and late phases was used to predict children's percent correct. These two predictors explained a significant proportion of the variance in children's behavioral performance ($R^2 = .25$, $F(2,22) = 3.68$, $p < .05$). The regression coefficients indicated that the pattern shown for 3-year-olds in Figure 8D was indicative of less skilled performance. In particular, a lower percent correct was predicted by a higher concentration of oxy-Hb in the early phase of SS3 trials ($\beta = -.18$, $p < .05$) and a lower concentration of oxy-Hb in the late phase of SS3 trials ($\beta = .13$, $p < .05$).

## 4. Discussion

VWM is a core cognitive system with severe capacity limitations that are predictive of individual differences in general cognitive processing (Gold et al., 2010). Recent studies using fMRI have revealed a frontal-parietal network that underlies VWM in both children and adults (e.g., Bunge & Wright, 2007; Edin et al., 2007; Fair et al., 2007; Geier et al., 2009; Klingberg et al., 2002; Klingberg, 2006; Kwon et al., 2002; Mitchell & Cusack, 2007; Nelson et al., 2000; Olesen et al., 2007; Scherf et al., 2006; Thomas et al., 1999; Todd & Marois, 2005; Todd, Fougnie, & Marois, 2005; Todd & Marois, 2004; Vuontela et al., 2009). The current study is the first to examine whether key signatures of this VWM system are evident in early development using fNIRS. In particular, we recorded functional neuroimaging data while 3- and 4-year-old children completed a change detection task—the method of choice for measuring the characteristics of VWM. Children showed severe capacity limits, consistent with previous work (see, e.g., Simmering, 2012). In particular, 3-year-olds showed a capacity of 1.3 items, and 4-year-olds showed a capacity of 1.8 items.

The first critical question we examined was whether the same frontal-parietal network identified in the fMRI literature would be evident here. Overall, there was good correspondence between frontal and parietal regions activated in prior studies and the robust neural responses measured here. Across all analyses, all 12 parietal channels showed a robust hemodynamic response for at least one age group, and there were robust hemodynamic responses in 4 left frontal channels and 1 right frontal channel. The parietal responses showed a canonical shape during the 12 s event window, with an increase in the concentration of oxy-Hb and a decrease in deoxy-Hb. The hemodynamic response in more lateral regions of the parietal cortex (P5) and in the left frontal cortex showed a different pattern, with an early increase in the concentration of oxy-Hb followed by a decrease in oxy-Hb and an increase in deoxy-Hb. This suggests a left-lateralized involvement in the early consolidation / maintenance of items in VWM, but may indicate that these regions play less of a role in the comparison phase. It is also notable that the frontal hemodynamic responses were much weaker in amplitude relative to the parietal responses. It is possible that this reflects the relative immaturity of the frontal cortex in early development (see, e.g., Moriguchi & Hiraki, 2009). The correspondence between robust parietal activation in early development and in adulthood is consistent with results from Cantlon and colleagues (2006). These researchers reported a strong correspondence between the hemodynamic responses of 4-year-olds and adults in the intraparietal sulcus in an event-related fMRI adaptation paradigm investigating numerical processing.

The second question we examined was whether the neural responses within the frontal-parietal network were sensitive to variation in working memory load (i.e., set size). This was indeed the case: four channels showed an increase in the concentration of oxy-Hb as the set size increased, with the highest concentrations at SS3. These results are not consistent with the adult VWM literature. In particular, several fMRI studies have reported an increase in the BOLD response as the set size increases with an asymptote in the neural signal for set sizes beyond the behavioral capacity limit. Children in the present study had a capacity that was less than 2 items. Nevertheless, there was a robust increase in the concentration of oxy-Hb up to SS3. This raises the intriguing possibility that the neural asymptote effect is a developmental achievement that emerges after 4 years of age.

Why might the concentration of oxy-Hb continue to increase beyond VWM capacity limits? One possibility is that neural responses for children at high set sizes are quite volatile. For instance, if children's ability to maintain WM representations is fragile (see Perone, Simmering, & Spencer, 2011; Simmering & Perone, 2013), it is possible that the presentation of the test array displaces some items in VWM, creating confusion as to which

items are old and which are new. Such volatility could drive a strong hemodynamic response given that the neuro-vascular response is sensitive to the overall change in excitatory and inhibitory influences (see Deco, Rolls, & Horwitz, 2004). Although this might explain our findings, it is notable that one channel—P4-1—showed a different pattern: an increase in the concentration of oxy-Hb up to SS2, with a weaker response at SS3. It is possible that this region of parietal cortex is more sensitive to capacity limitations; however, once again, it is important to note that we did not find the asymptotic pattern.

The final question we examined was how the frontal-parietal VWM network changes in early development. Overall, 4-year-olds tended to show more robust parietal responses relative to 3-year-olds, and a greater sensitivity to the working memory demands. By contrast, 3-year-olds showed an increase in the concentration of oxy-Hb in the early phase and a decrease in oxy-Hb in the late phase in both left parietal and right frontal cortex. Notably, the pattern in right frontal cortex was predictive of poorer behavioral performance. This suggests that over development, children who effectively engage the right frontal cortex during the *latter* portion of the event window and *increase* the concentration of oxy-Hb perform the task more accurately. This may point to an emerging role for the right frontal cortex over development in the comparison phase of the task.

Note that although our fNIRS data are compelling, several issues must be resolved in future work. First, we used the same probe geometry for all children in the present study with a 3 cm distance between sources and detectors (see Boas, Dale, & Franceschini, 2004). Using the same probe geometry across children controlled the optical path length, but this may not be optimal because children vary in head circumference and brain anatomy. Consequently, we could be recording from slightly different anatomical locations across participants. Moreover, other physiological / physical changes over development can impact the fNIRS signal including skull thickness, changes in surface tissues, and differences in systematic physiology. Such differences might have impacted how the fNIRS signal changed over development. For instance, 4-year-olds showed a robust increase in the concentration of oxy-Hb in the left parietal cortex as the set size increased, while 3-year-olds did not (see Figure 8B–8C). Future work combining fNIRS and structural MRI would clarify whether this developmental difference reflects a functional reorganization of parietal cortex between these ages or a change in underlying brain anatomy / physiology (for an examination of related issues with adults, see Cooper et al., 2012).

Finally, it is important to acknowledge that our sample was slightly under-powered in some conditions. Moreover, we did not explicitly control the false discovery rate using, for instance, a Bonferoni correction. A recent analysis by Barker, Aarabi, and Huppert (2013) shows that standard fMRI analysis techniques yield a high false-positive rate when applied to fNIRS data. Thus, at present it is unclear how to control the false discovery rate in fNIRS analyses (although see Barker et al., 2013 for an innovative approach). This issue prevents us from drawing strong conclusions from our results. Nevertheless, the current data make an important contribution to the literature, providing key initial findings that can help guide future work in this area. One technical point is whether the average across participants should be performed on the concentration changes or on the changes normalized by the standard error. The former provides a grand average estimate of the concentration changes, but this could be biased by individual participants with noisy results. The latter overcomes this by averaging a t-statistic across participants, but this loses information about the physiological amplitude of the evoked response. When one is only interested in whether a significant activation occurs at a given location and not a physiological interpretation of the amplitude of the response, then averaging of the t-statistic is the preferred choice. However, if the noise across subjects is fairly uniform, as was the case in the present study, then both approaches will lead to comparable results.

In summary, the present study was the first functional neuroimaging study to examine the neural basis of VWM capacity in early development. We demonstrated that fNIRS can be an effective tool to probe the frontal-parietal network that underlies VWM, detecting variations in this network as key task demands (i.e., memory load) are manipulated. Moreover, we revealed several striking changes in the VWM network over development and raised the possibility that a central neural signature of VWM capacity revealed in studies of adults may be a developmental achievement that emerges after 4 years of age.

## Acknowledgments

This is the first study reporting data collected using the Delta Center's CHILDS (CHild Imaging Laboratory in Development Science) facility. Thus, we would like to thank the Office of the Executive Vice President and Provost, the Office of the Vice President for Research, the College of Liberal Arts and Sciences, the Department of Psychology, and the Department of Communication Sciences and Disorders at the University of Iowa for their generous support. In addition, we thank the CHILDS facility Director—Larissa Samuelson—for her immense assistance, Qianqian Fang for generating the digitized image of the head used herein, Jay Dubb for assistance with Homer2, and Vincent Magnotta for consultation on the fNIRS analyses. Sammy Perone, Sobana Wijeakumar, and Kevin Bohache provided helpful comments on earlier versions of this manuscript. Finally, we thank the parents and children who participated in the study, and the undergraduate research assistants in the SPAM lab. DAB acknowledges support from NIH P41-14075. Note that DAB is an inventor on a technology licensed to TechEn, a company whose medical pursuits focus on noninvasive, optical brain monitoring. DAB's interests were reviewed and are managed by Massachusetts General Hospital and Partners HealthCare in accordance with their conflict of interest policies.

## References

Alloway TP. Working memory, reading, and mathematical skills in children with developmental coordination disorder. Journal of experimental child psychology. 2007; 96(1):20–36. [PubMed: 17010988]

Aslin D, Mehler J. Near-infrared spectroscopy for functional studies of brain activity in human infants: Promise, prospects, and challenges. Journal of Biomedical Optics. 2005; 10(011009):1–4.

Barker JW, Aarabi A, Huppert TJ. Autoregressive model based algorithm for reducing the effects of motion artifacts and serially correlated errors in functional near infrared spectroscopic imaging. 2013 Manuscript submitted for publication.

Boas DA, Gaudette T, Strangman G, Cheng X, Marota JJ, Mandeville JB. The accuracy of near infrared spectroscopy and imaging during focal changes in cerebral hemodynamics. NeuroImage. 2001; 13(1):76–90. [PubMed: 11133311]

Boas, David A.; Dale, AM.; Franceschini, MA. Diffuse optical imaging of brain activation: approaches to optimizing image sensitivity, resolution, and accuracy. NeuroImage. 2004; 23(Suppl 1):S275–S288. [PubMed: 15501097]

Bunge, Sa; Wright, SB. Neurodevelopmental changes in working memory and cognitive control. Current opinion in neurobiology. 2007; 17(2):243–250. [PubMed: 17321127]

Cantlon JF, Brannon EM, Carter EJ, Pelphrey Ka. Functional imaging of numerical processing in adults and 4-y-old children. PLoS biology. 2006; 4(5):e125. [PubMed: 16594732]

Conway ARA, Kane MJ, Engle RW. Working memory capacity and its relation to general intelligence. Trends in cognitive sciences. 2003; 7(12):547–552. Retrieved from http://www.ncbi.nlm.nih.gov/pubmed/14643371. [PubMed: 14643371]

Cooper RJ, Caffini M, Dubb J, Fang Q, Custo A, Tsuzuki D, Fischl B, et al. Validating atlas-guided DOT: a comparison of diffuse optical tomography informed by atlas and subject-specific anatomies. NeuroImage. 2012; 62(3):1999–2006. [PubMed: 22634215]

Cowan N, Elliott EM, Saults JS, Morey CC, Mattox S, Hismjatullina A, Conway ARA. On the capacity of attention: Its estimation and its role in working memory and cognitive aptitudes. Cognitive Psychology. 2005; 51:42–100. [PubMed: 16039935]

Cui X, Bray S, Reiss AL. Functional near infrared spectroscopy (NIRS) signal improvement based on negative correlation between oxygenated and deoxygenated hemoglobin dynamics. NeuroImage. 2010; 49(4):3039–3046. [PubMed: 19945536]

Cullen AE, Dickson H, West SA, Morris RG, Mould GL, Hodgins S, Murray RM, et al. Neurocognitive performance in children aged 9–12 years who present putative antecedents of schizophrenia. Schizophrenia research. 2010; 121(1–3):15–23. [PubMed: 20580530]

Cutini S, Scarpa F, Scatturin P, Jolicœur P, Pluchino P, Zorzi M, Dell'Acqua R. A hemodynamic correlate of lateralized visual short-term memories. Neuropsychologia. 2011; 49(6):1611–1621. [PubMed: 21163274]

Deco G, Rolls ET, Horwitz B. "What" and "Where" in visual working memory: A computational neurodynamical perspective for integrating fMRI and single-neuron data. Journal of Cognitive Neuroscience. 2004; 16:683–701. [PubMed: 15165356]

Edin F, Macoveanu J, Olesen P, Tegnér J, Klingberg T. Stronger synaptic connectivity as a mechanism behind development of working memory-related brain activity during childhood. Journal of cognitive neuroscience. 2007; 19(5):750–760. [PubMed: 17488202]

Fair DA, Dosenbach NU, Church JA, Cohen AL, Brahmbhatt S, Miezin FM, Barch DM, Raichle ME, Petersen SE, Schlaggar BL. Development of distinct control networks through segregation and integration. Acad Proc Natl Sci U.S.A. 2007; 104(33):13507–13512.

Fukuda K, Vogel E, Mayr U, Awh E. Quantity, not quality: the relationship between fluid intelligence and working memory capacity. Psychonomic bulletin & review. 2010; 17(5):673–679. [PubMed: 21037165]

Geier CF, Garver K, Terwilliger R, Luna B. Development of working memory maintenance. Journal of neurophysiology. 2009; 101(1):84–99. [PubMed: 18971297]

Gold JM, Hahn B, Zhang WW, Robinson BM, Kappenman ES, Beck VM, Luck SJ. Reduced capacity but spared precision and maintenance of working memory representations in schizophrenia. Archives of general psychiatry. 2010; 67(6):570–577. [PubMed: 20530006]

Green, SB.; Salkind, NJ.; Akey, TM. Using SPSS for Windows: Analyzing and Understanding Data. New Jersey: Prentice Hall; 1997.

Harris, RJ. A Primer of Multivariate Statistics: 2nd Edition. New York, NY: Academic Press; 1985.

Harrison A, Jolicoeur P, Marois R. "What" and "where" in the intraparietal sulcus: an FMRI study of object identity and location in visual short-term memory. Cerebral Cortex. 2010; 20(10):2478–2485. [PubMed: 20100899]

Heckman JJ. Skill formation and the economics of investing in disadvantaged children. Science (New York, N.Y.). 2006; 312(5782):1900–1902.

Howell, DC. Statistical Methods for Psychology. Boston, MA: PWS-Kent Publishing; 1992.

Huppert TJ, Hoge RD, Diamond SG, Franceschini MA, Boas DA. A temporal comparison of BOLD, ASL, and NIRS hemodynamic responses to motor stimuli in adult humans. NeuroImage. 2006; 29(2):368–382. [PubMed: 16303317]

Huppert, Theodore J.; Diamond, SG.; Franceschini, MA.; Boas, DA. HomER: a review of time-series analysis methods for near-infrared spectroscopy of the brain. Applied Optics. 2009; 48(10):1–33. [PubMed: 19107163]

Klingberg T. Development of a superior frontal-intraparietal network for visuo-spatial working memory. Neuropsychologia. 2006; 44(11):2171–2177. [PubMed: 16405923]

Klingberg T, Forssberg H, Westerberg H. Increased brain activity in frontal and parietal cortex underlies the development of visuospatial working memory capacity during childhood. Journal of cognitive neuroscience. 2002; 14(1):1–10. [PubMed: 11798382]

Kwon H, Reiss AL, Menon V. Neural basis of protracted developmental changes in visuo-spatial working memory. Proceedings of the National Academy of Sciences of the United States of America. 2002; 99(20):13336–13341. [PubMed: 12244209]

Lloyd-Fox S, Blasi A, Elwell CE. Illuminating the developing brain: the past, present, and future of functional near infrared spectroscopy. Neuroscience and Biobehavioral Reviews. 2010; 34:269–284. [PubMed: 19632270]

Luck SJ, Vogel EK. The capacity of visual working memory for features and conjunctions. Nature. 1997; 390:279–281. [PubMed: 9384378]

Luck S, Vogel E. The capacity of visual working memory for features and conjunctions. Nature. 1997; 390(6657):279–281. [PubMed: 9384378]

Mitchell DJ, Cusack R. Flexible, capacity-limited activity of posterior parietal cortex in perceptual as well as visual short-term memory tasks. Cerebral Cortex. 2007; 18:1788–1798. [PubMed: 18042643]

Moriguchi Hiraki KY. Neural origin of cognitive shifting in young children. PNAS. 2009; 106(14): 6017–6021. [PubMed: 19332783]

Nęcka E. Cognitive analysis of intelligence: The significance of working memory processes. Personality and Individual Differences. 1992; 13(9):1031–1046.

Nelson CA, Monk CS, Lin J, Carver LJ, Thomas KM, Truwit CL. Functional neuroanatomy of spatial working memory in children. Developmental Psychology. 2000; 36:109–116. [PubMed: 10645748]

Oakes, LM.; Horst, JS.; Kovack-Lesh, KA.; Perone, S. Learning and the infant mind. New York: Oxford University Press; 2008. How Infants Learn Categories; p. 144-171.

Olesen PJ, Macoveanu J, Tegnér J, Klingberg T. Brain activity related to orking memory and distraction in children and adults. Cerebral cortex (New York, N.Y. : 1991). 2007; 17(5):1047–1054.

Pashler H. Familiarity and visual change detection. Perception & Psychophysics. 1988; 44:369–378. [PubMed: 3226885]

Perone S, Simmering VR, Spencer JP. Stronger neural dynamics capture changes in infants' visual working memory capacity over development. Developmental science. 2011; 14(6):1379–1392. [PubMed: 22010897]

Pessoa L, Gutierrez E, Bandettini P, Ungerleider LG. Neural correlates of visual working memory: fMRI amplitude predicts task performance. Neuron. 2002; 35(5):975–987. [PubMed: 12372290]

Pessoa L, Ungerleider L. Neural correlates of change detection and change blindness in a working memory task. Cerebral Cortex. 2004; 14:511–520. [PubMed: 15054067]

Riggs KJ, McTaggart J, Simpson A, Freeman RPJ. Changes in the capacity of visual working memory in 5- to 10-year-olds. Journal of Experimental Child Psychology. 2006; 95:18–26. [PubMed: 16678845]

Roche-Labarbe, N.; Fenoglio, A.; Radhakrishnan, H.; Kocienski-Filip, M.; Carp, Sa; Dubb, J.; Boas, Da, et al. Somatosensory evoked changes in cerebral oxygen consumption measured non-invasively in premature neonates. NeuroImage. 2013. http://dx.

Rose SA, Feldman JF, Jankowski JJ. Information Processing in Toddlers: Continuity from Infancy and Persistence of Preterm Deficits. Intelligence. 2009; 37(3):311–320. [PubMed: 20161244]

Rose SA, Feldman JF, Jankowski JJ. Implications of Infant Cognition for Executive Functions at Age 11. Psychological science. 2012; 23(11):1345–1355. [PubMed: 23027882]

Scherf KS, Sweeney JA, Luna B. Brain basis of developmental change in visuospatial working memory. Journal of cognitive neuroscience. 2006; 18(7):1045–1058. [PubMed: 16839280]

Schroeter ML, Zysset S, Wahl M, Von Cramon DY. Prefrontal activation due to Stroop interference increases during development--an event-related fNIRS study. NeuroImage. 2004; 23(4):1317–1325. [PubMed: 15589096]

Seghier ML, Lazeyras F, Huppi PS. Functional MRI of the newborn. Seminars in Fetal Neonatal Medicine. 2006; 11:479–488. [PubMed: 17000141]

Simmering VR, Perone S. Working memory as a dynamic process. Frontiers. 2013; 3:1–26.

Simmering, Vanessa R. The development of visual working memory capacity during early childhood. Journal of experimental child psychology. 2012; 111(4):695–707. [PubMed: 22099167]

Steele SD, Minshew NJ, Luna B, Sweeney JA. Spatial working memory deficits in autism. Journal of autism and developmental disorders. 2007; 37(4):605–612. [PubMed: 16909311]

Thomas KM, King SW, Franzen PL, Welsh TF, Berkowitz a L, Noll DC, Birmaher V, et al. A developmental functional MRI study of spatial working memory. NeuroImage. 1999; 10(3 Pt 1): 327–338. [PubMed: 10458945]

Todd, Marois RJJ. Posterior parietal cortex activity predicts individual differences in visual short-term memory capacity. Cognitive, Affective, & Behavioral Neuroscience. 2005; 5(2):144–155.

Todd Fougnie D, Marois RJJ. Visual short-term memory load suppresses temporo-parietal junction activity and induces inattentional blindness. Psychological Science. 2005; 16(12):965–972. [PubMed: 16313661]

Todd JJ, Marois R. Capacity limit of visual short-term memory in human posterior parietal cortex. Nature. 2004; 428:751–754. [PubMed: 15085133]

Vicari S, Caravale B, Carlesimo GA, Casadei AM, Allemand F. Spatial working memory deficits in children at ages 3–4 who were low birth weight, preterm infants. Neuropsychology. 2004; 18(4): 673–678. [PubMed: 15506835]

Vogel EK, Woodman GF, Luck SJ. Storage of features, conjunctions, and objects in visual working memory. Journal of Experimental Psychology: Human Perception and Performance. 2001; 27:92–114. [PubMed: 11248943]

Vuontela V, Steenari M-R, Aronen ET, Korvenoja A, Aronen HJ, Carlson S. Brain activation and deactivation during location and color working memory tasks in 11–13-year-old children. Brain and cognition. 2009; 69(1):56–64. [PubMed: 18620789]

Willcutt EG, Doyle AE, Nigg JT, Faraone SV, Pennington BF. Validity of the executive function theory of attention-deficit/hyperactivity disorder: a meta-analytic review. Biological psychiatry. 2005; 57(11):1336–1346. [PubMed: 15950006]

Wolf M, Greisen G. Advances in near-infrared spectroscopy to study the brain of the preterm and term neonate. Clinics in Perinatology. 2009; 36:807–834. [PubMed: 19944837]

## Highlights

- This manuscript presents data from the first functional neuroimaging study to examine the neural basis of visual working memory capacity in early development.
- We show for the first time that functional near-infrared spectroscopy can be used to detect task-specific variations in the frontal-parietal network that underlies visual working memory abilities.
- Children did not show an asymptote in the amplitude of the neural signal at their visual working memory capacity limit as seen with adults; thus, the asymptote effect may be a developmental achievement that emerges after the age of 4 years.
- Four-year-olds show a broader engagement of the parietal cortex and more sensitivity to the working memory load.

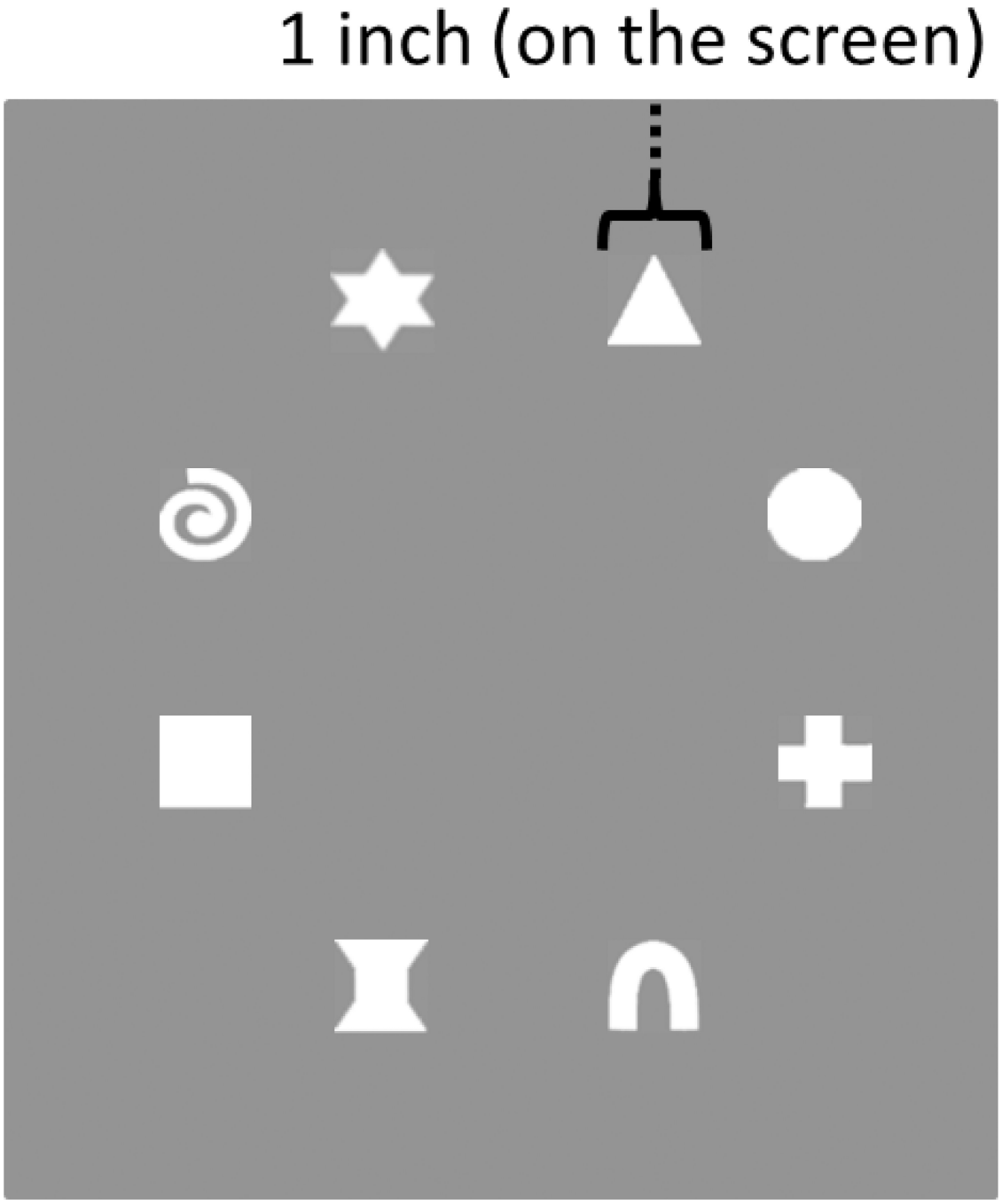


**Figure 1.**
The eight white shapes used in the change detection task.

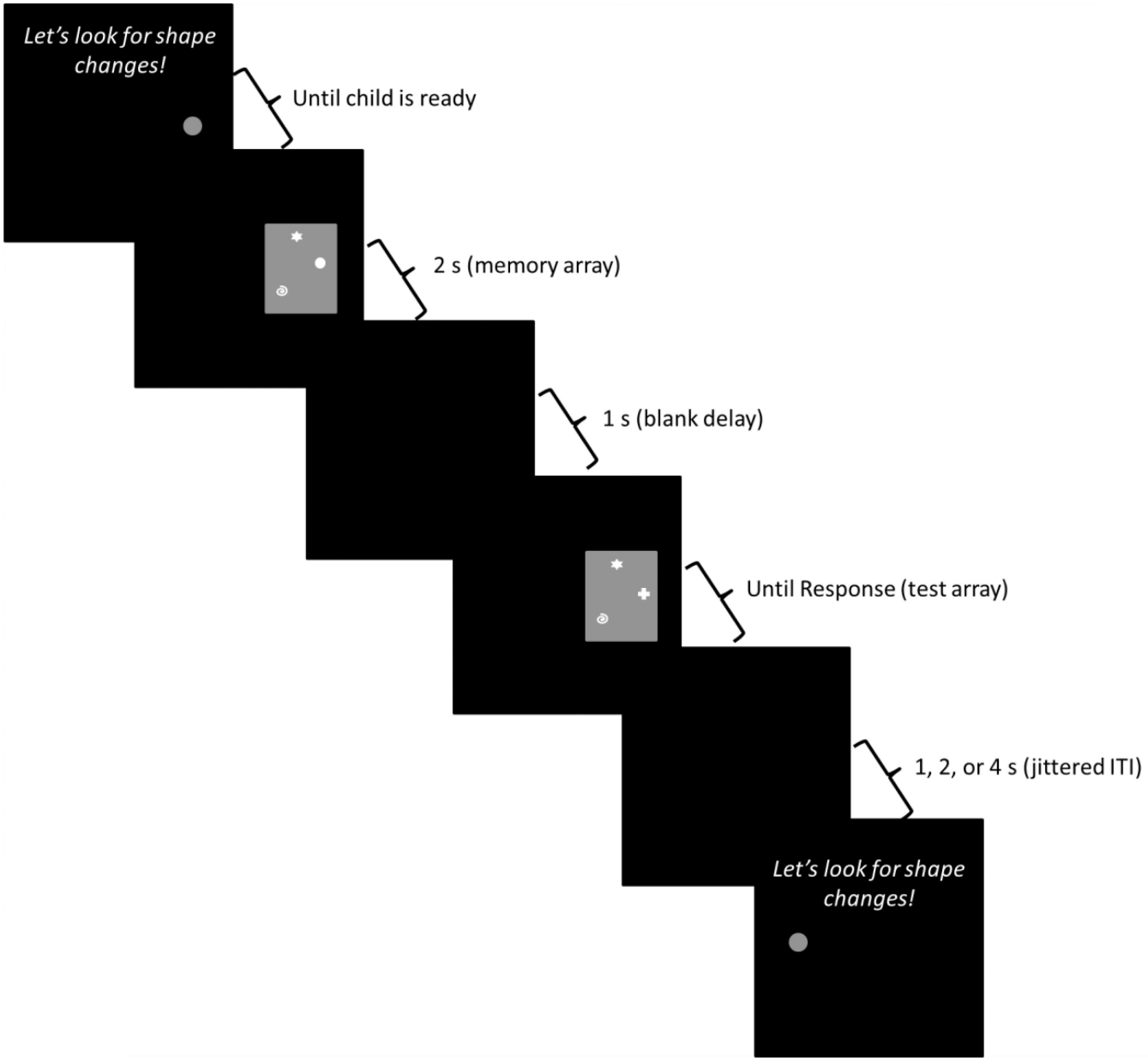


**Figure 2.**

Sequence of events during a trial. Each trial began with an auditory prompt saying, "Let's look for shape changes!" along with a fixation circle on the left or right side of the screen. The experimenter initiated the trial when the child was ready. The sample array then appeared on the screen for 2 s, followed by a blank interval of 1 s. The test array was then presented until the child verbally responded 'match' or 'no-match'. The experimenter entered the child's response on a keyboard. After a jittered inter-trial interval of either 1, 2, or 4 s, the next trial was presented on the other side of the screen. This example shows a 'different' trial at SS3 (the circle in the sample array changes to a plus-sign in the test array).


**Figure 3.**
Child performing the task while wearing the fNIRS cap.

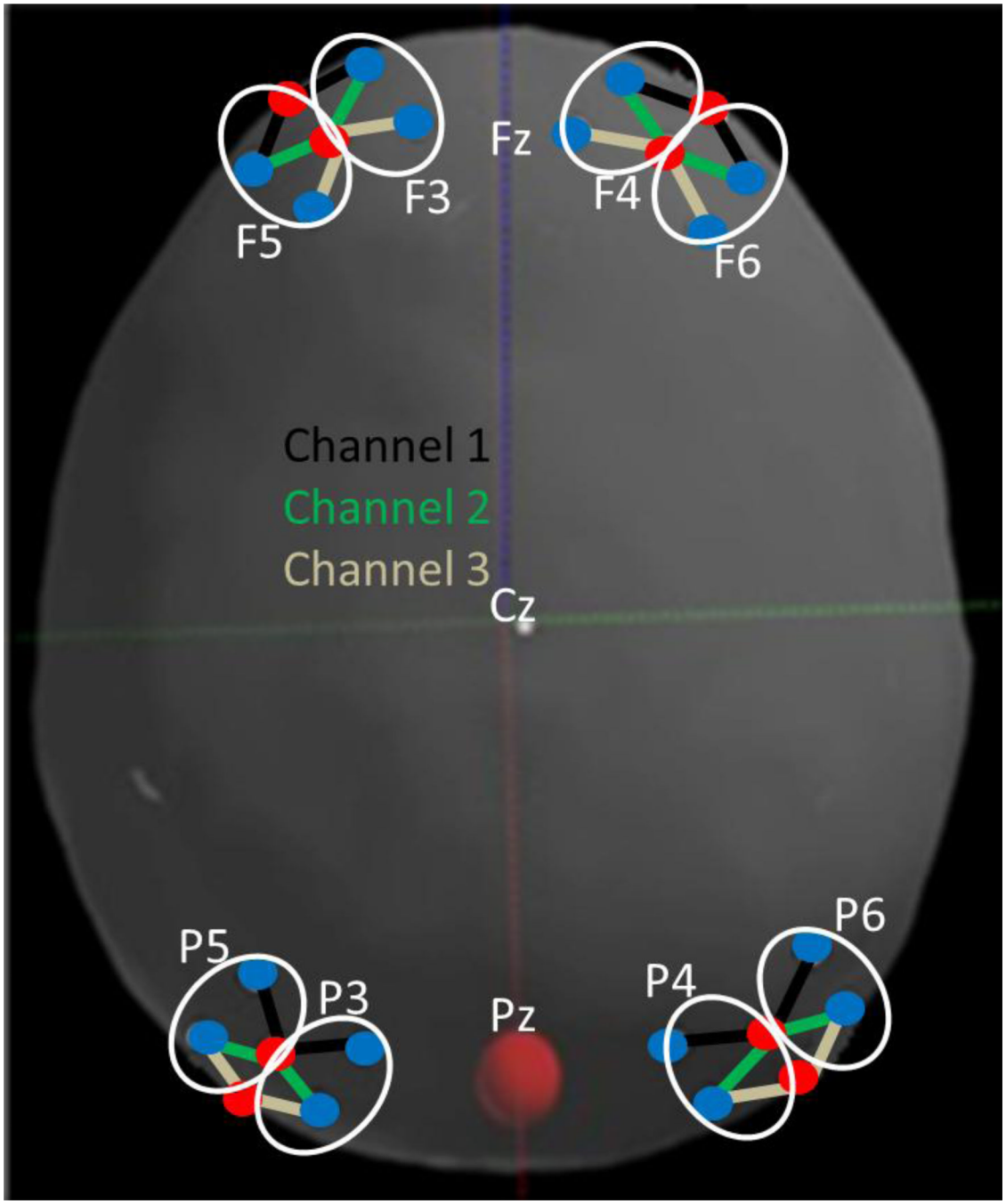


**Figure 4.**

The locations of the fNIRS probes in relation to landmarks in the 10–20 system. Sources are marked with red circles; detectors are marked with blue circles. Data channels are defined as a connection between a source and a detector. Channels are referred to by their position in the 10–20 system (see white ovals) and a channel number (1, 2, or 3 moving from front to back). For instance, F5-1 is the yellow channel near F5, F5-2 is the purple channel, and F5-3 is the green channel.

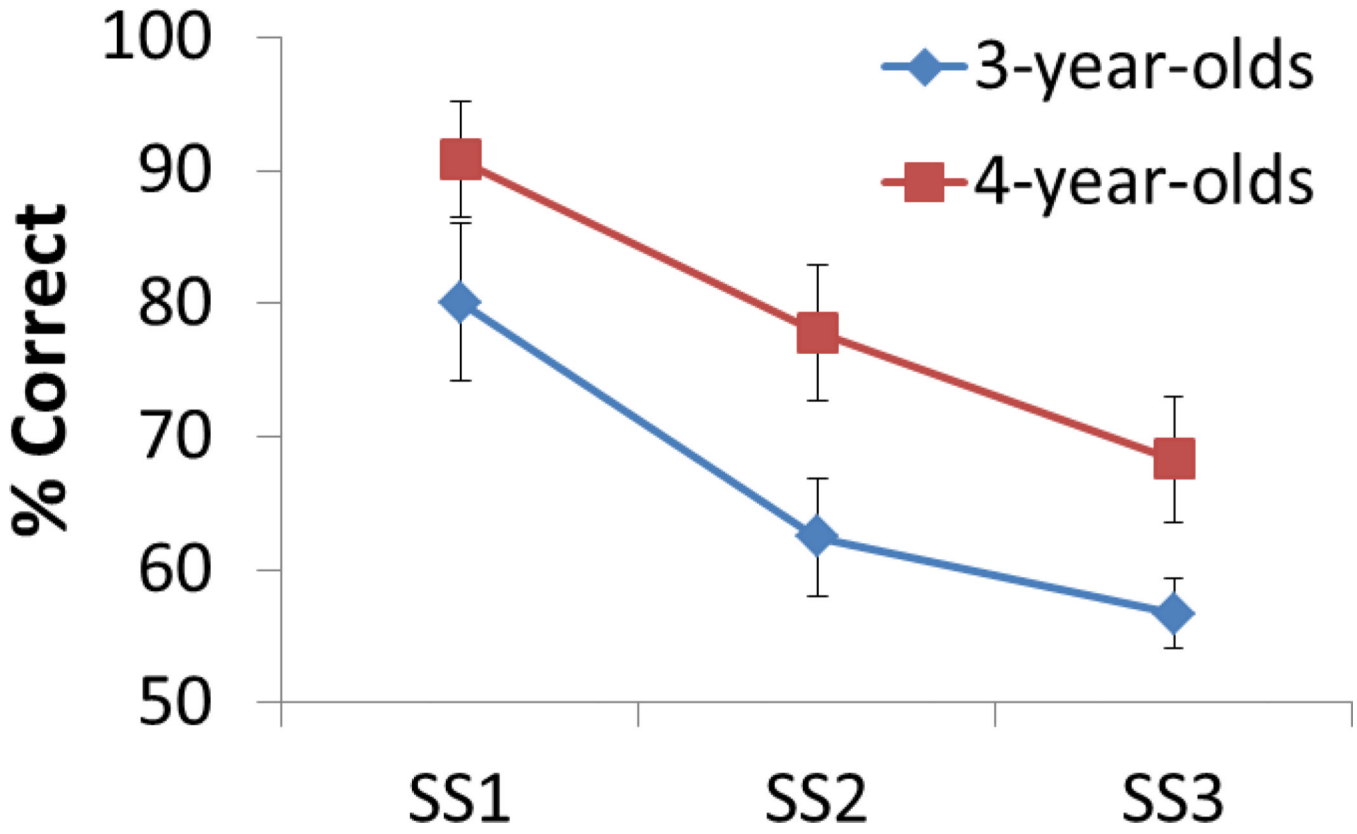


**Figure 5.**
Children's behavioral performance (percent correct) as the set size (SS) varied from 1 to 3 items. Error bars show 1 *SD*.

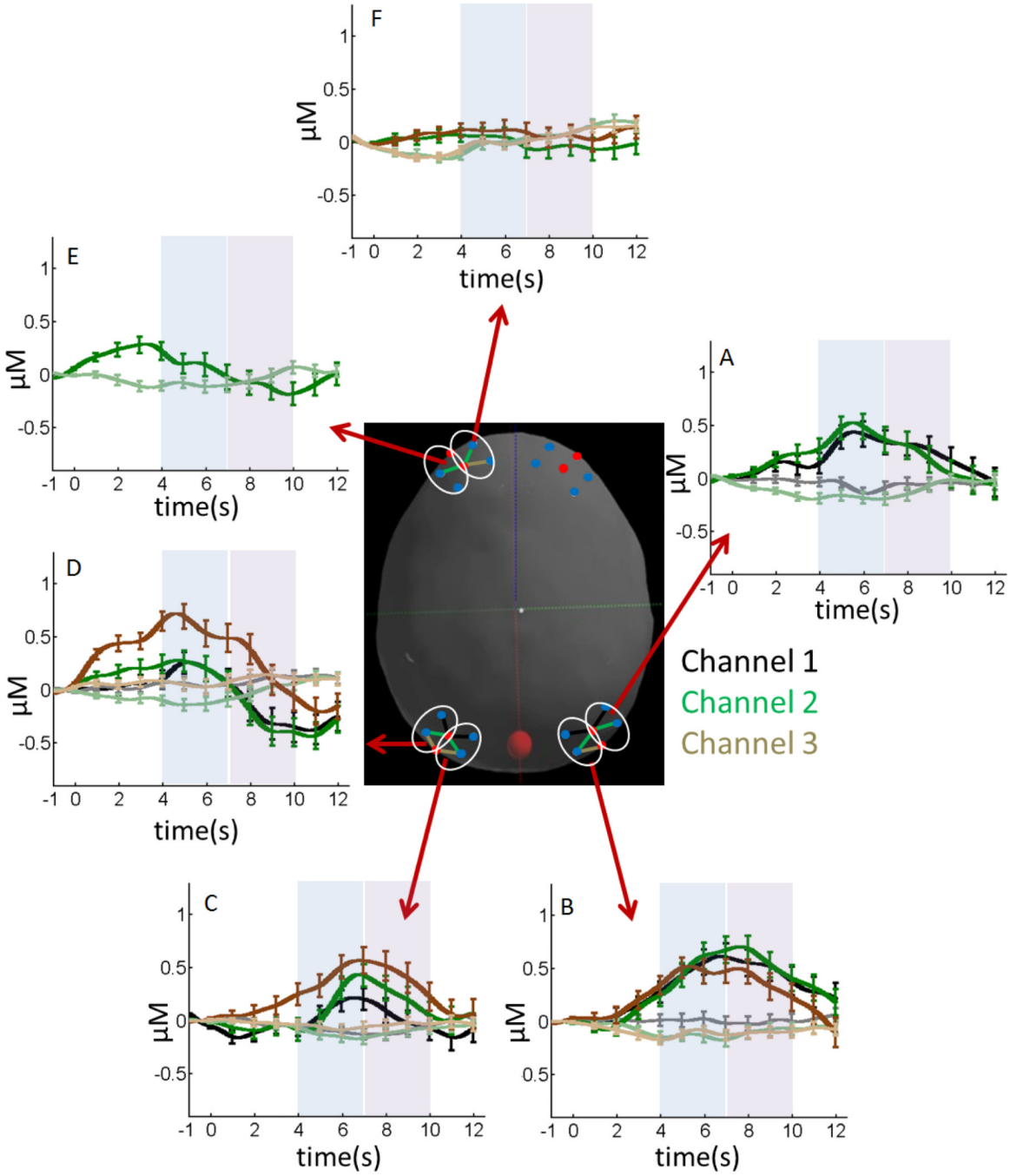


**Figure 6.**

Concentrations of oxy-Hb (dark colors) and deoxy-Hb (light colors) for fNIRS channels showing a difference in the concentration of these chromophores during the early phase (4–7 s; see blue shaded time window) or late phase (7–10 s; see magenta shaded time window). The center image shows the selected fNIRS channels. The color of these channels matches the dark-light color pairs in each panel (e.g., dark green line in panel A shows oxy-Hb for channel P6-2; light green line shows deoxy-Hb). Error bars show 1 SE averaged over 1 s intervals.

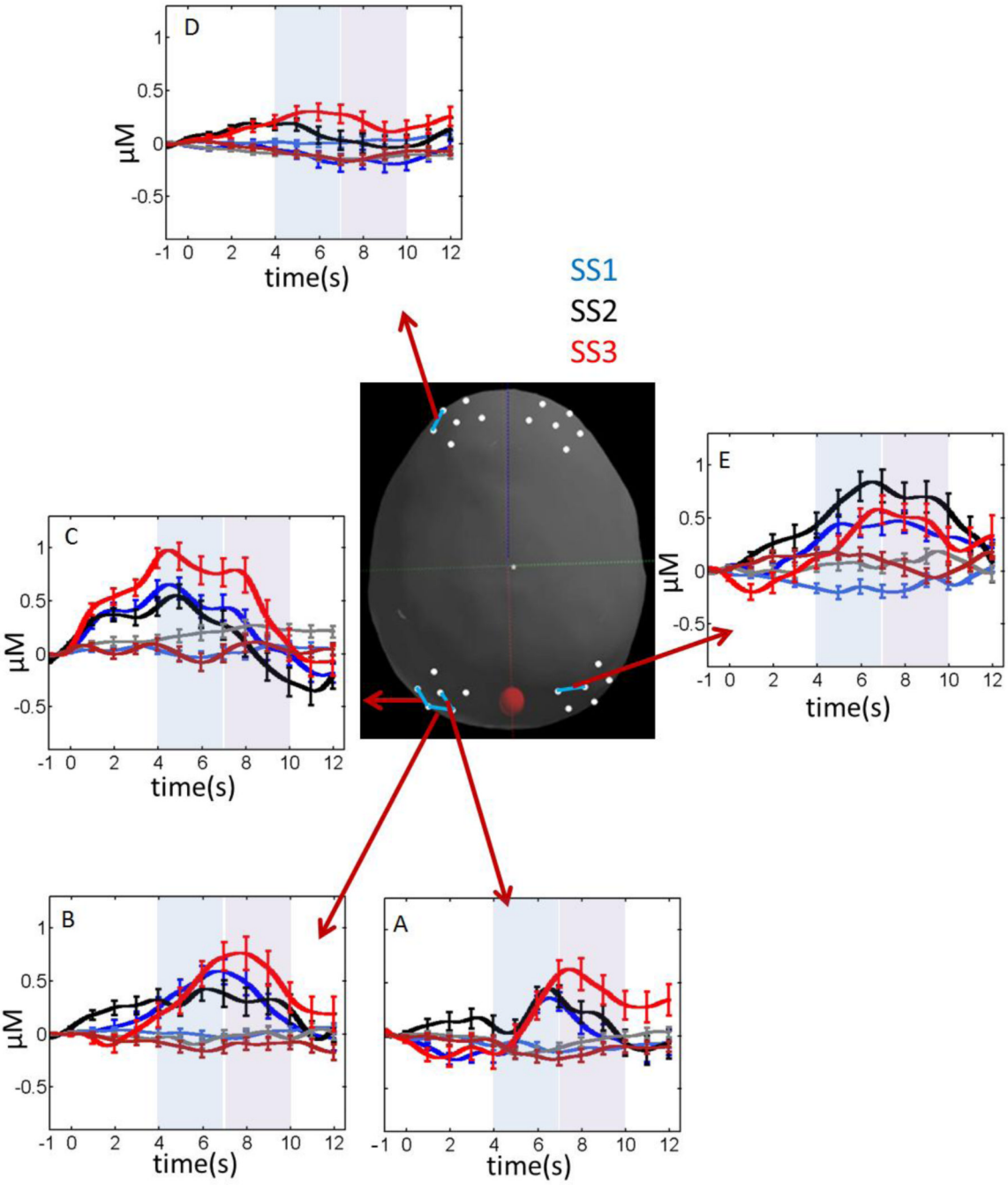


**Figure 7.**

Concentrations of oxy-Hb (dark colors) and deoxy-Hb (light colors) for fNIRS channels showing robust set size (SS) effects. Blue lines = SS1; black lines = SS2; red lines = SS3. The center image shows the selected fNIRS channel depicted in each panel. Error bars show 1 SE averaged over 1 s intervals.

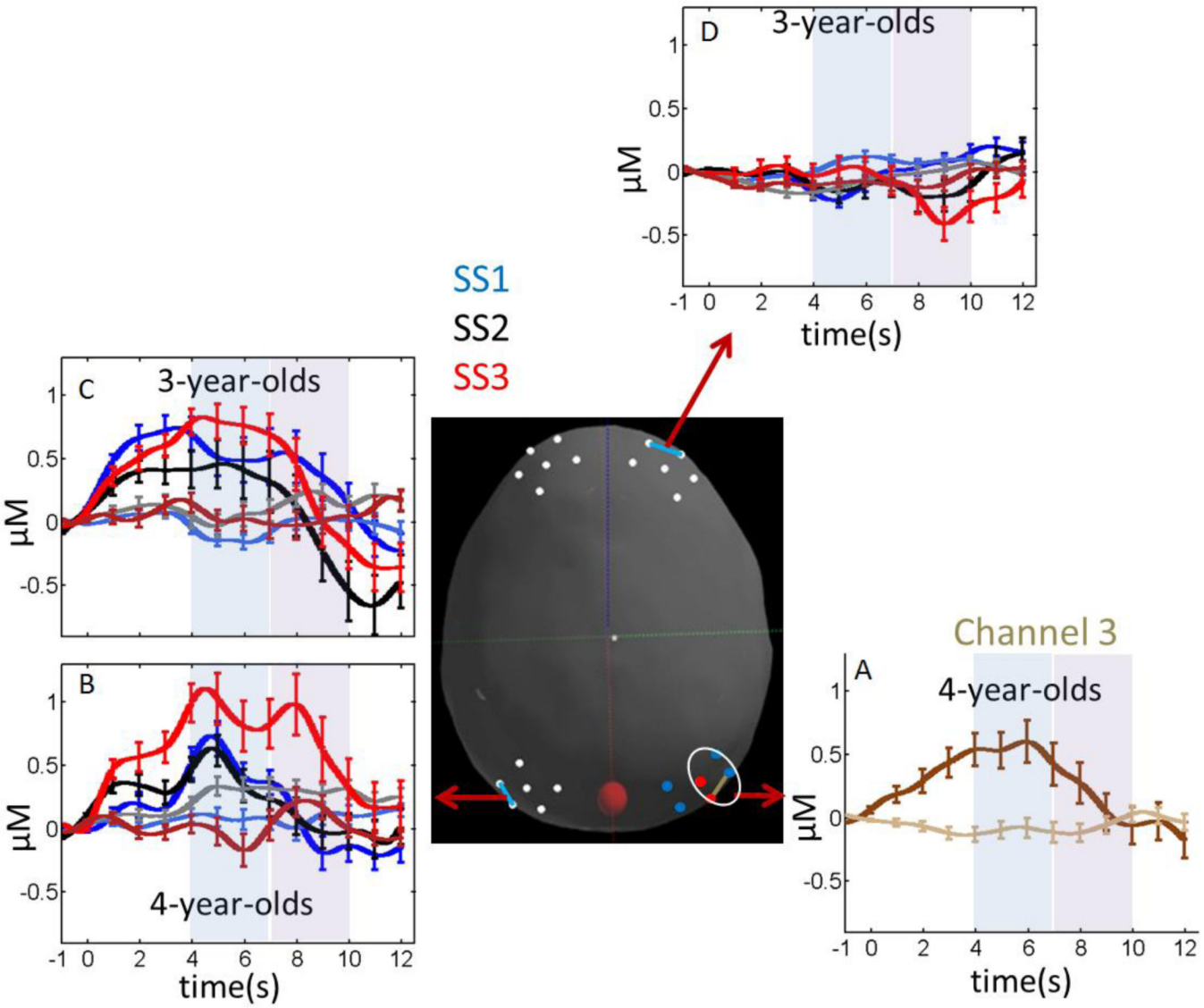


**Figure 8.**

Concentrations of oxy-Hb (dark colors) and deoxy-Hb (light colors) for fNIRS channels showing robust Age effects. Brown color in panel A follows the colors scheme from Figure 6 (dark brown = oxy-Hb; light brown = deoxy-Hb). Colors in panels B, C, and D follow the color scheme from Figure 7: blue lines = SS1; black lines = SS2; red lines = SS3. The center image shows the selected fNIRS channel depicted in each panel. Error bars show 1 SE averaged over 1 s intervals.

**Table 1**

Number of participants (N), trial counts (correct trials only), and percentage of trials (in parentheses) included within each region, age, and set-size.

| | | | Average Correct Trial Count (% included) | | | |
|---|---|---|---|---|---|---|
| **Age** | **Region** | **N** | **SS1** | **SS2** | **SS3** | **Grand Avg** |
| 3-yo | F3 | 12 | 23 (*80*) | 19 (*80*) | 17 (*74*) | 20 (*78*) |
| | F4 | 13 | 26 (*90*) | 21 (*89*) | 18 (*87*) | 22 (*89*) |
| | F5 | 12 | 26 (*84*) | 21 (*87*) | 19 (*84*) | 22 (*85*) |
| | F6 | 14 | 25 (*84*) | 20 (*81*) | 17 (*79*) | 21 (*81*) |
| | P3 | 11 | 25 (*78*) | 19 (*77*) | 17 (*77*) | 20 (*77*) |
| | P4 | 7 | 22 (*69*) | 17 (*67*) | 14 (*70*) | 19 (*69*) |
| | P5 | 11 | 20 (*65*) | 17 (*66*) | 15 (*66*) | 17 (*66*) |
| | P6 | 12 | 21 (*69*) | 17 (*63*) | 13 (*63*) | 17 (*65*) |
| 4-yo | F3 | 13 | 22 (*67*) | 20 (*72*) | 18 (*70*) | 20 (*70*) |
| | F4 | 12 | 26 (*82*) | 23 (*81*) | 20 (*78*) | 23 (*80*) |
| | F5 | 15 | 22 (*69*) | 19 (*67*) | 18 (*69*) | 20 (*68*) |
| | F6 | 12 | 23 (*69*) | 20 (*66*) | 16 (*62*) | 20 (*66*) |
| | P3 | 16 | 22 (*64*) | 18 (*59*) | 15 (*55*) | 18 (*59*) |
| | P4 | 13 | 19 (*60*) | 17 (*58*) | 14 (*52*) | 17 (*57*) |
| | P5 | 13 | 22 (*67*) | 19 (*63*) | 14 (*57*) | 18 (*62*) |
| | P6 | 17 | 20 (*64*) | 17 (*61*) | 15 (*58*) | 18 (*61*) |

**Table 2**

fNIRS channels with significant HbX ($HbO_2 \neq HbR$), Phase (Early ≠ Late), or HbX × Phase interactions that did not also interact with set size or age.

| Omnibus ANOVA | | | Tests of Simple Effects (HbX × Phase) | | |
|---|---|---|---|---|---|
| **Channel** | **Effect** | $F(df_{effect}, df_{error})$ | **Early:$HbO_2$>HbR** | **$HbO_2$:Early>Late** | **HbR:Late>Early** |
| P3-1 | HbX | $F(1,25) = 6.00^{*}$ | | | |
| P3-2 | HbX | $F(1,25) = 4.99^{*}$ | | | |
| P3-3 | HbX | $F(1,25) = 7.70^{**}$ | | | |
| P4-1 | HbX | $F(1,18) = 7.34^{*}$ | | | |
| P4-2 | HbX | $F(1,18) = 20.51^{***}$ | | | |
| P4-3 | HbX | $F(1,18) = 14.98^{***}$ | | | |
| P5-1 | Phase | $F(1,22) = 5.22^{*}$ | | | |
| | HbX × Phase | $F(1,22) = 11.54^{**}$ | $F(1,22) = 1.93$ | $F(1,22) = 11.1^{**}$ | $F(1,22) = 0.95$ |
| P5-2 | Phase | $F(1,22) = 6.78^{*}$ | | | |
| | HbX × Phase | $F(1,22) = 25.14^{***}$ | $F(1,22) = 4.77^{*}$ | $F(1,22) = 16.4^{***}$ | $F(1,22) = 6.61^{*}$ |
| P5-3 | HbX × Phase | $F(1,22) = 14.51^{***}$ | $F(1,22) = 15.1^{***}$ | $F(1,22) = 9.02^{**}$ | $F(1,22) = 1.93$ |
| P6-1 | HbX | $F(1,27) = 7.35^{*}$ | | | |
| P6-2 | HbX | $F(1,27) = 7.97^{**}$ | | | |
| | HbX × Phase | $F(1,27) = 5.85^{*}$ | $F(1,27) = 11.3^{**}$ | $F(1,27) = 0.08$ | $F(1,27) = 0.10$ |
| F3-2 | HbX × Phase | $F(1,23) = 8.88^{**}$ | $F(1,23) = 0.12$ | $F(1,23) = 2.16$ | $F(1,23) = 5.92^{*}$ |
| F3-3 | HbX × Phase | $F(1,23) = 6.43^{*}$ | $F(1,23) = 2.46$ | $F(1,23) = 0.86$ | $F(1,23) = 4.86^{*}$ |
| F5-2 | HbX × Phase | $F(1,25) = 6.42^{*}$ | $F(1,25) = 0.74$ | $F(1,25) = 5.33^{*}$ | $F(1,25) = 3.53$ |

$^{*}p < .05$;

$^{**}p < .01$;

$^{***}p < .001$

## Table 3

fNIRS channels with significant set size effects.

| Channel | Effect | $F(df_{effect}, df_{error})$ |
|---|---|---|
| P3-2 | SS × Phase | $F(2,24) = 3.52^{*}$ |
| | SS × Phase × HbX | $F(2,24) = 3.57^{*}$ |
| P3-3 | SS × Phase | $F(2,24) = 3.84^{*}$ |
| P4-1 | SS | $F(2,17) = 3.89^{*}$ |
| P5-3 | SS × HbX | $F(2,21) = 5.56^{*}$ |
| F5-1 | SS × HbX | $F(2,24) = 5.65^{**}$ |

$^{*}p < .05$;

$^{**}p < .01$

Note: all channels reported here met the criterion for inclusion in fNIRS analyses, that is, these channels exhibited a significant HbX ($HbO_2 \neq HbR$) effect (either a main effect or interaction).

## Table 4

fNIRS channels with significant age effects.

| Channel | Effect | $F(df_{effect}, df_{error})$ |
|---|---|---|
| P3-1 | Age | $F(1,25) = 4.87^{*}$ |
| P5-3 | Age × SS × Phase | $F(2,21) = 8.38^{**}$ |
| P6-3 | Age × Phase | $F(1,27) = 5.81^{*}$ |
| | Age × Phase × HbX | $F(1,27) = 5.41^{*}$ |
| F4-1 | SS × Phase | $F(2,22) = 6.26^{**}$ |
| | SS × Phase × HbX | $F(2,22) = 4.88^{*}$ |
| | SS × Phase × HbX × Age | $F(2,22) = 4.22^{*}$ |

$^{*}p < .05$;

$^{**}p < .01$

Note: all channels reported here met the criterion for inclusion in fNIRS analyses, that is, these channels exhibited a significant HbX ($HbO_2 \neq HbR$) effect (either a main effect or interaction).